Hydrol. Earth Syst. Sci., 29, 5477–5491, 2025 https://doi.org/10.5194/hess-29-5477-2025 © Author(s) 2025. This work is distributed under the Creative Commons Attribution 4.0 License.





Time shift between precipitation and evaporation has more impact on annual streamflow variability than the elasticity of potential evaporation

Vazken Andréassian¹, Guilherme Mendoza Guimarães¹, Alban de Lavenne¹, and Julien Lerat²

¹Université Paris-Saclay, INRAE, HYCAR Research Unit, Antony, France

Correspondence: Vazken Andréassian (vazken.andreassian@inrae.fr)

Received: 3 February 2025 – Discussion started: 14 February 2025

Revised: 1 July 2025 - Accepted: 1 September 2025 - Published: 21 October 2025

Abstract. One of the most basic questions asked of hydrologists is the quantification of catchment response to climatic variations, i.e., the variations around the average annual flow given the climatic anomaly of a particular year. This paper presents an analysis based on 4122 catchments from four continents, where we investigate how annual streamflow variability depends on climate variables – rainfall and potential evaporation - and on the synchronicity between precipitation and potential evaporation. We use catchment data to verify the existence of this link and show that, in all countries and under the main climates represented, anomalies in this synchronicity are the second most important factor to explain annual streamflow anomalies, after precipitation, but before potential evaporation. Introducing the synchronicity between precipitation and potential evaporation as an independent variable improves the prediction of annual streamflow variability with an average additional explained variance of 6 % globally.

Notations. We deal in this paper with three hydrological fluxes: precipitation (P_n) , streamflow (Q_n) and potential evaporation (E_{0n}) . The three fluxes are computed at catchment scale, expressed in millimeters per year, and represent annual totals (index n refers to the year in question). We use a hydrological year from 1 October of year n-1 to 30 September of year n in the Northern hemisphere and from 1 April of year n to 31 March of year n+1 in the Southern hemisphere. Anomalies (of P, Q and E_0), noted Δ , are computed as the difference between the annual value and the long-term average value, i.e., $\Delta Q_n = Q_n - \bar{Q}$, $\Delta P_n = P_n - \bar{P}$, etc.

1 Introduction

1.1 On the climate elasticity of streamflow

To assess the impact of climate change on water resources, hydrologists aim to quantify the amount of change in catchment flow when climatic conditions vary. The ratio between changes in streamflow and climate is formally defined as the climate elasticity of streamflow (Schaake and Liu, 1989). The hydrological literature and common sense both suggest that the best factor explaining the changes in annual streamflow is the annual precipitation anomaly (e.g., Pardé, 1933a; Leopold, 1974). In addition, many elasticity studies have also considered the anomaly of potential evaporation, although it is usually only weakly statistically significant in regression studies. In this paper, we focus on a third explanatory variable that quantifies the synchronicity between precipitation and potential evaporation within the year.

1.2 Linear models to predict streamflow anomalies

There is an abundance of literature concerning elasticity studies in hydrology, and our work builds upon the earlier empirical (i.e., measurement-based) studies of Sankarasubramanian et al. (2001), Chiew (2006), and Andréassian et al. (2016). Here, we follow the same principle and use linear regression models based on measured annual data to evaluate the climate elasticity of streamflow. An alternative approach to estimating climate elasticities would involve using hydrological models of varying complexities (e.g., Koster and Suarez, 1999). However, even if models are powerful inves-

²CSIRO, Canberra, Australia

tigative tools, they also rely on restrictive assumptions that often limit their credibility outside their calibration range. This can be particularly problematic in a large-scale study on the impact of climate change. Thus, we favored an approach introducing the minimal number of hydrological assumptions, hence a linear regression that also has the advantage of being mathematically extremely simple.

1.3 The synchronicity between precipitation and potential evaporation impacts annual streamflow totals

The fact that the time shift between precipitation and potential evaporation, hereon referred to as "climatic synchronicity", has a hydrological impact has been known for a long time, as shown by a few precursors on this topic. For example, Pardé (1933b) published a classic paper dedicated to the average flow of rivers, where he underlined that "for identical values of precipitation and temperature, everything else being equal, the runoff coefficient Q/P will be smaller where the larger part of precipitation falls during the warm season". Similarly, Coutagne and de Martonne (1935) discussed formulas for annual streamflow, and underlined that formulas based only on the humidity ratio P/E_0 are deficient, because they fail to account for "the distribution of precipitations between seasons, in particular, in the temperate zone, between the warm and the cold season. Of two years of equal precipitation, the year which will receive the most part in summer will produce the less annual flow". Additional classical studies include Thornthwaite (1948), who proposed to classify climates initially with two indices (one characterizing the periods of water surplus and the other the periods of water deficiency), which he subsequently combined into a single index. A few years later, Turc (1954) introduced his famous formula for long-term actual evaporation. At the very end of his paper, he wrote that "the most urgent improvement" to his actual evaporation formula should be the introduction of the "distribution of precipitations and of the temperature changes within the year."

Recent studies have also discussed the impact of climate seasonality on water balance, based on either theoretical or empirical approaches. Among the theoretical studies, Dooge (1992) presented catchment yield curves where he introduced as a parameter the length of the dry season. Milly (1994) proposed a theoretical computation of actual evaporation based on the seasonality of the aridity index. Yokoo et al. (2008) made theoretical computations on the difference between in-phase and out-of-phase regimes of precipitation and potential evapotranspiration. Additionally, Roderick and Farquhar (2011), Feng et al. (2012), Donohue et al. (2012), Berghuijs et al. (2014) and Jawitz et al. (2022) all made notable developments. Among the empirical studies, Potter et al. (2005) quantified the impact of rainfall seasonality on mean annual water balance in Australia. Hickel and Zhang (2006) discussed the antagonistic effects of climate seasonality and soil moisture storage. More recently, de Lavenne and Andréassian (2018) proposed a synchronicity index to characterize the phase difference between precipitation and potential evaporation, and Feng et al. (2019) proposed an index of asynchronicity for Mediterranean climates.

1.4 Purpose of the paper

In this paper, we aim to improve the prediction of streamflow elasticity by introducing anomalies in synchronicity between precipitation and potential evaporation as a predictor, alongside variability in rainfall and potential evapotranspiration. Our study is based solely on data analysis, and uses only linear regression models.

2 Test catchments

2.1 Origin of the dataset

As presented in Table 1, we use catchments from nine countries to base our analysis on a wide range of climates.

The total number of catchments is 4122, for a total of 162 005 station-years (the average length of catchment time series is 39 years). We use hydrological years as defined in the Notations section.

2.2 Catchment selection

The catchments used in this paper were selected from several datasets indicated in Table 1 and represent approximately 75 % of the original catchments. Our catchment selection was based on three criteria: record length, catchment memory and regulation degree. First, we only selected catchments that had more than 20 complete hydrological years. Second, we selected catchments that exhibit minimal interannual memory ("memory" as defined by de Lavenne et al., 2022). This criterion was needed because the equation used here to estimate streamflow elasticity is only hydrologically warranted for catchments displaying minimum interannual memory, thus allowing a straightforward computation of annual elasticity coefficients, based only on annual average values. Finally, catchments identified as significantly regulated by reservoirs were removed. This identification was done by either asking the datasets authors, or, where the information was available, by setting a limit equal to 10 mm equivalent volume storage in dams). For Switzerland, the list of almost natural catchments published by Muelchi et al. (2022) was utilized.

2.3 Climatic inputs

Where several precipitation products were available in the original dataset, we used the product recommended by dataset authors as being of the best quality, while avoiding precipitation data based exclusively on satellite estimates.

Table 1. Origin of the catchments used in this paper.

Country	Number of catchments selected	Number of catchments available in the original dataset	Dataset	Reference
Australia	546	561	Camels-AUS	Fowler et al. (2025)
Brazil	636	734	Cabra	Almagro et al. (2021)
Denmark	202	304	Camels-DK	Liu et al. (2025)
France	628	654	Camels-FR	Delaigue et al. (2025)
Germany	1094	1555	Camels-DE	Loritz et al. (2024)
Sweden	152	158	Selection by Göran Lindström	de Lavenne et al. (2022)
Switzerland	73	331	Camels-CH	Höge et al. (2023)
United Kingdom	136	670	Camels-UK	Coxon et al. (2020)
USA	655	672	Camels-US	Addor et al. (2017)

In the original datasets, potential evaporation was computed with a variety of different formulas (Makkink, Morton, FAO-56, Penman-Monteith, Hargreaves, Oudin, etc.). For the sake of homogeneity, we recomputed it (at the daily time step) for all catchments using the formula proposed by Oudin et al. (2005), which requires only extraterrestrial radiation and air temperature. This formula was selected for two reasons: first, it could be computed, given the available data, for all datasets, and it has been widely used worldwide and appears appropriate (while of course not perfect) for describing atmospheric evaporative demand.

2.4 Characteristics of the catchment set

In our dataset, the aridity index, computed as E_0/P , ranges from 0.1 to 6.3, with a first quartile of 0.6 and a third quartile of 1.0. The mean and the median of the aridity index are both 0.8. In order to assess the generality of the results, we will discuss them at the country scale and also by climatic classes following the Köppen-Geiger classification (see e.g., Peel et al. 2007 and Table 2). Note that we only give numerical results for the climatic zones with more than 100 catchments.

Finally, Fig. 1 presents the 4122 catchments of our dataset with two variants of the Turc-Budyko non-dimensional graph. On the left-hand graph, each catchment corresponds to one point, with coordinates representing the average aridity on the x-axis and "actual evaporation" yield, computed as (P-Q)/P, on the y-axis. On the right-hand graph, each catchment is represented by a single point, with coordinates indicating the average humidity on the x-axis and the average streamflow yield, computed as Q/P, on the y-axis.

3 Method

3.1 Computation of the synchronicity of precipitation and potential evaporation

In this paper, we utilize a modified version of the seasonality index introduced by de Lavenne and Andréassian (2018): a detailed discussion of the reasons for this change is provided in Appendix A. The objective of this index (Λ) is to characterize the synchronicity between precipitation P and potential evaporation E_0 at the annual time step. For each year n, we define the part of annual precipitation that is the most easily accessible to evaporation (i.e., neutralizable by evaporation) as in Eq. (1) and Fig. 2:

synchronous
$$P - E_0$$
 amount $= \sum_{m=1}^{12} \min(P_{m,n}, E_{0_{m,n}})$ (1)

where the index m refers to the calendar month.

The percentage of easily neutralizable precipitation is then defined as Eq. (2), and the percentage of easily neutralizable potential evaporation as Eq. (3).

$$\lambda_{1,n} = \frac{\sum_{m=1}^{12} \min(P_{m,n}, E_{0_{m,n}})}{P_n}$$
 (2)

$$\lambda_{2,n} = \frac{\sum_{m=1}^{12} \min(P_{m,n}, E_{0_{m,n}})}{E_{0_n}}$$
 (3)

Because both ratios belong to the interval [0,1], their geometric average will also be within the same range (Eq. 4).

$$\lambda_{3,n} = \sqrt{\lambda_{1,n}\lambda_{2,n}} = \frac{\sum_{m=1}^{12} \min(P_{m,n}, E_{0_{m,n}})}{\sqrt{P_n E_{0_n}}}$$
(4)

Finally, the index Λ rescales and combines λ_1 and λ_2 into a single quantity, expressed in mm yr⁻¹, representing the average ratio of neutralizable precipitation and neutralizable potential evaporation as shown in Eq. (5). For two years with the same annual amounts of precipitation and potential evaporation, Λ will reach higher values when P and E_0 are synchronous, and lower values when they are out of phase.

$$\Lambda_n = \lambda_{3,n} \cdot \bar{P} = \frac{\sum_{m=1}^{12} \min(P_{m,n}, E_{0_{m,n}})}{\sqrt{P_n \cdot E_{0_n}}} \cdot \bar{P}$$
 (5)

Table 2. Main climatic zones (in the sense of the Köppen-Geiger classification) represented in our dataset (we present the zones counting more than 100 catchments).

Köppen-Geiger zone	Name	Number of catchments
Aw	Tropical savanna climate with dry winter	344
Cfa	Temperate climate without dry season with hot summer	364
Cfb	Temperate climate without dry season with warm summer	1746
Csa	Temperate climate with dry and hot summers	196
Dfb	Continental climate without dry season with warm summer	956
Dfc	Continental climate without dry season with cold summer	132

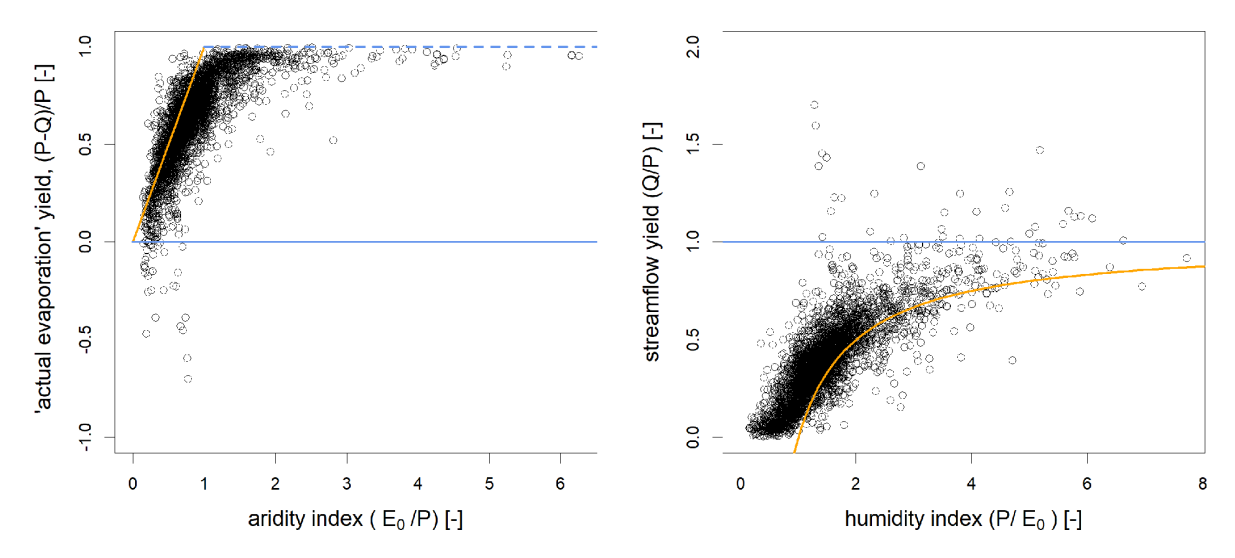


Figure 1. Representation of the 4122 catchments in two equivalent forms of the Turc-Budyko non-dimensional space. The solid blue line corresponds to the water limit (Q = P), and the orange line corresponds to the energy limit ($Q = P - E_0$). On the left, an additional limit (dotted blue line) is sometimes improperly referred to as "water limit" in the literature, but it only corresponds to the physical limit (Q = 0, when one estimates the actual evaporation as the difference between discharge and precipitation. The catchments that are beyond the orange line (i.e., above on the left and below on the right) are "leaky" (in the sense that they contribute to the recharge of a regional aquifer) and those which are beyond the blue line (i.e., below on the left and above on the right) are "gaining" in the sense of a karstic catchment which would drain a larger than specified catchment (note that in a few cases, data uncertainties might also cause catchments to be beyond the limits).

3.2 Computation of streamflow elasticities

To compute the streamflow elasticities, we solve two linear equations given by Eqs. (6) and (7).

$$\Delta Q_n = e_{Q/P} \Delta P_n + e_{Q/E_0} \Delta E_{0_n} \tag{6}$$

$$\Delta Q_n = e_{Q/P} \Delta P_n + e_{Q/E_0} \Delta E_{0_n} + e_{Q/\Lambda} \Delta \Lambda_n \tag{7}$$

Where ΔQ_n (respectively ΔP_n , ΔE_{0_n} , $\Delta \Lambda_n$) represents the deviation from the mean annual value (anomaly) for variable Q (respectively P, E_0 , Λ) in mm yr $^{-1}$ and $e_{Q/P}$, e_{Q/E_0} and $e_{Q/\Lambda}$ represent the elasticity of streamflow with respect to P, E_0 , and Λ (dimensionless).

Equation (6) represents the classical approach to elasticity computation (Andréassian et al., 2016), while Eq. (7) represents the original contribution of this paper, and aims at

determining how far climatic synchronicity explains annual streamflow variability.

The elasticities in Eqs. (6) and (7) are estimated via ordinary least squares (OLS). More complex statistical models such as generalized least squares are not required because the selected catchments do not exhibit interannual memory, as explained in the data section. This absence of interannual memory guarantees the lack of autocorrelation in annual streamflow, which is an important statistical assumption for OLS. Additionally, we chose a p-value threshold of 0.05 for all the discussion of results. We compute elasticity coefficients between anomalies of equal dimensions (in mm yr⁻¹), and not between relative anomalies (in %) because with the anomalies expressed in mm yr⁻¹ the physically-plausible range is known: [0,1] for $e_{O/P}$, [-1,0] for e_{O/E_0} and $e_{O/\Lambda}$.

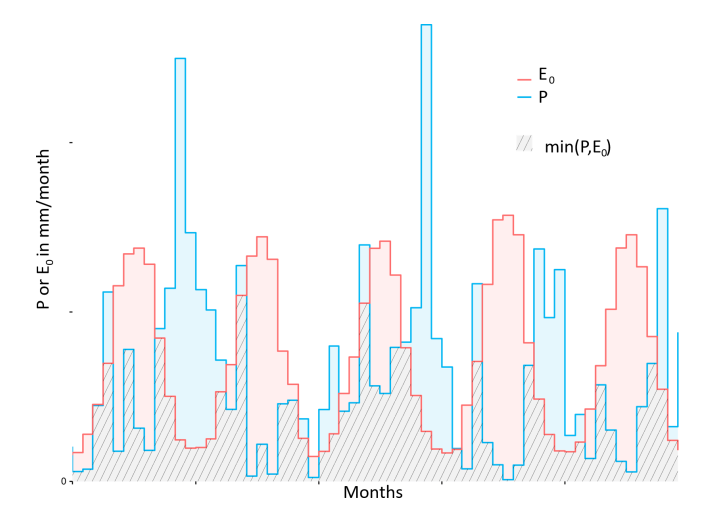


Figure 2. Two series of precipitation and potential evaporation at catchment scale: the part of precipitation that is the most easily accessible to evaporation is illustrated in hatched pattern.

Finally, Eqs. (6) and (7) were solved on a catchment-by-catchment basis, i.e., we computed 4122 distinct regressions.

Figure 3 illustrates this catchment-based computation using the example of the Meurthe River at Raon-l'Étape (727 km²). For this catchment, annual streamflow anomalies exhibit a well-defined dependency on both precipitation and synchronicity anomalies, with the dependency on potential evaporation anomaly being very weak.

The visual impression of Fig. 3 is confirmed by the results of the linear regressions of Eqs. (6) and (7) in Table 3. Values of the Student's t-test indicate that precipitation has a dominant contribution, while the contribution of potential evaporation is not statistically significant. The introduction of synchronicity increases the R^2 from 0.75 to 0.80.

4 Results

4.1 Graphical analysis of anomalies by country

To provide a general overview of the correlation between streamflow anomalies and climatic anomalies, Figs. 4 and 5 present an aggregated plot for each country and for each main climate class, combining the anomalies of all catchments. At this scale, only general trends are apparent. As expected, streamflow anomaly is clearly positively correlated with precipitation anomaly in all countries; streamflow anomaly is, overall, very weakly negatively correlated with potential evaporation anomaly, Denmark being the only outlier with a weak positive correlation (it is mainly due to the year 1990, which was a very dry year in Denmark, but with an unusual cold summer). Streamflow anomaly is clearly negatively correlated to the synchronicity index anomaly (Λ) for all countries. This negative correlation indicates that years with a lower Λ (i.e., when precipitation and potential evaporation

are more out of phase) yield greater streamflow. This observation is perfectly hydro-logical, and conforms to general observations previously identified by Pardé (1933a). In the case of Australia, where streamflow anomalies are clearly negatively correlated to the synchronicity index anomaly (Λ) on Fig. 4, it is interesting to mention the opposite conclusion of Potter et al. (2005) who wrote that "the inclusion of seasonally varying forcing alone was not sufficient to explain variability in the mean annual water balance". This surprising conclusion may be an artefact of the index chosen by the authors to describe seasonality.

Overall, the most surprising fact is that streamflow anomaly appears more strongly correlated with the synchronicity index anomaly than with the potential evaporation anomaly.

4.2 Overall results by catchment

We now analyze the results obtained for each of the 4122 catchments. Table 4 shows the statistics of the individual regressions for the classical case when synchronicity is not included as a predictor. This analysis reveals that for all countries and all climate groups, the precipitation elasticity of streamflow is almost always significant at the 0.05 level. On the other hand, the potential evaporation elasticity of streamflow is not frequently significant at the 0.05 level. In addition, the regression identifies physically realistic precipitation elasticity values (between 0 and 1) for almost all catchments (93 % worldwide, and a minimum of 80 % across different groupings), whereas potential evapotranspiration elasticity is frequently physically unrealistic with only 6 % of values in the range [0,1] globally.

Table 5 presents the same statistics, when the synchronicity anomaly $(\Delta \Lambda_n)$ is introduced into the elasticity regression (Eq. 7). This analysis shows that the average efficiency of the regression equation increases across all countries and climate groups (see also Fig. 6). While an increase is expected when an additional predictor is added to a regression, please note that we are presenting adjusted R^2 values, which are designed to take that issue into account. The average additional explained variance lies in the range 3%-10% (6% globally), depending on the group, and we consider it a noticeable improvement. Additionally, the synchronicity anomaly $(\Delta \Lambda_n)$ provides a significant contribution to the regression for 64% of the catchments, compared to only 23% for potential evaporation).

More important, the introduction of the synchronicity anomaly $(\Delta \Lambda_n)$ does not modify the significance of the other two elasticity coefficients $e_{Q/P}$ and e_{Q/E_0} . A slight increase is observed in the proportion of catchments where e_{Q/E_0} coefficient is significant at the 0.05 level (from 16% to 23%). Moreover, the utilization of $\Delta \Lambda_n$ does not degrade the physical realism of the elasticity coefficients $e_{Q/P}$ and e_{Q/E_0} . Once again, a slight increase is observed in the proportion of catchments where $e_{Q/P}$ coefficient is significant and in the

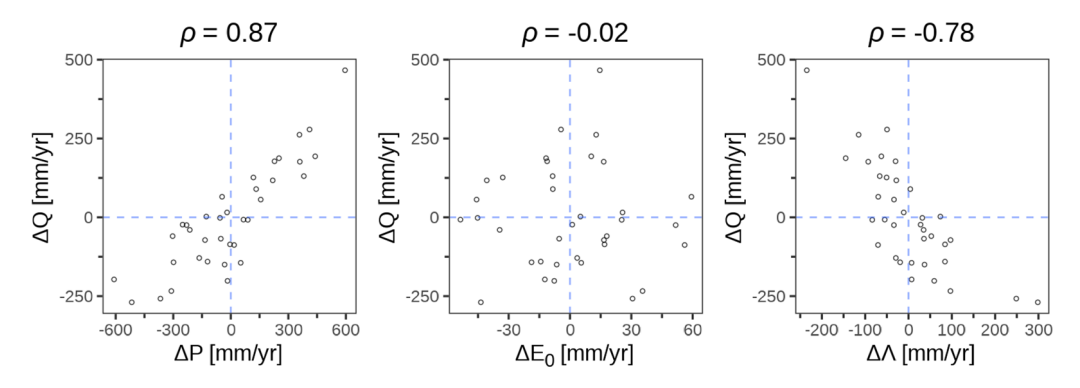


Figure 3. Example of an elasticity plot for the Meurthe River at Raon-l'Étape (A615103001): each point corresponds to one hydrological year (for this catchment, 36 hydrological years were available, from 1975 to 2021). The Pearson correlations of ΔQ with ΔP , ΔE_0 and $\Delta \Lambda$ are respectively 0.87, -0.02 and -0.78.

Table 3. Climate elasticity coefficients computed with and without the inclusion of the synchronicity variable Λ for the example catchment (La Meurthe at Raon-l'Étape).

Formulation	$e_{Q/P}$ [-]	p -value for $e_{Q/P}$	e_{Q/E_0} [–]	p -value for e_{Q/E_0}	$e_{Q/\Lambda}$ [-]	p -value for $e_{Q/\Lambda}$	R^2
$\Delta Q = f(\Delta P, \Delta E_0)$ $\Delta Q = f(\Delta P, \Delta E_0, \Delta \Lambda)$	0.52 0.38	< 0.001 < 0.001	0.00 -0.25	0.99 0.59		< 0.01	0.75

physical range [0,1] (from 93 % to 94 %), and where e_{Q/E_0} coefficient is significant at the 0.05 level and in the physical range [-1,0] (from 6 % to 11 %). Finally, only two countries (Switzerland and Brazil) and one climate type (Dfc – Continental climate without dry season with cold summer) showed lower relevance of the synchronicity index compared to other regions. We attribute this reduced relevance in Switzerland and climate zone Dfc to the essentially energy-limited nature of the catchments as our selection criteria for Switzerland prioritized high-elevation catchments with minimal anthropogenic impact (see also the Discussion section and Fig. 9). Last, note that in all groupings except Dfc, the number of catchments where $e_{Q/\Lambda}$ is significant at the 0.05 level exceeds that where the e_{Q/E_0} coefficient is significant at the same level.

5 Discussion

Figure 6 illustrates the improvement in explanatory capacity of the regressions due to the introduction of the synchronicity anomalies. While considerable variability exists, and some catchments show equivalent performance between the two regression models (indicated by points on the 1:1 line), the graph confirms that for many catchments (approximately 66 % of the dataset, where $e_{Q/\Lambda}$ was significant at the 0.05 level), accounting for synchronicity anomalies visibly improves the efficiency of the linear regression. Because the adjusted R^2 shows the same trend as the classical R^2 , this is clearly not a simple effect of the increase of independent variables in the regression.

In Fig. 7, we summarize the significance of the $e_{Q/\Lambda}$ coefficient across all the Köppen climate classes represented in our dataset: $e_{Q/\Lambda}$ is significant at the 0.05 level for 50% of the catchments in 11 classes (representing 79% of the catchments).

Figure 8 shows the geographic distribution of the catchments where the $P-E_0$ synchronicity had a significant contribution to explain streamflow anomalies (with a p-value threshold of 0.05). The map brings further elements to Table 5 and illustrates that there are sub-regions where the coefficient $e_{Q/\Lambda}$ is mostly not significant at the 0.05 level. Based on our knowledge of the climatic specificities of each country, this seems to be possibly correlated to higher rainfall (cf. the Danish dataset, with the particular behavior of the West of Jutland, the case of Florida in the US, the case of the Scottish catchments in Great Britain) and/or to colder areas (cf. the Swiss, Swedish and US datasets).

To verify this hypothesis, Fig. 9 presents the p-values of the $4122\,e_{Q.\Lambda}$ coefficients as a function of the humidity index P/E_0 . This graph clearly indicates that most of the humid catchments (Humidity index > 2) lack sensitivity to the $P-E_0$ seasonality, and this pattern is likely the main explanation for the geographical patterns observed in Fig. 8.

6 Conclusions

6.1 Synthesis

In this paper, we investigated the dependency between streamflow elasticity and the synchronicity of precipitation

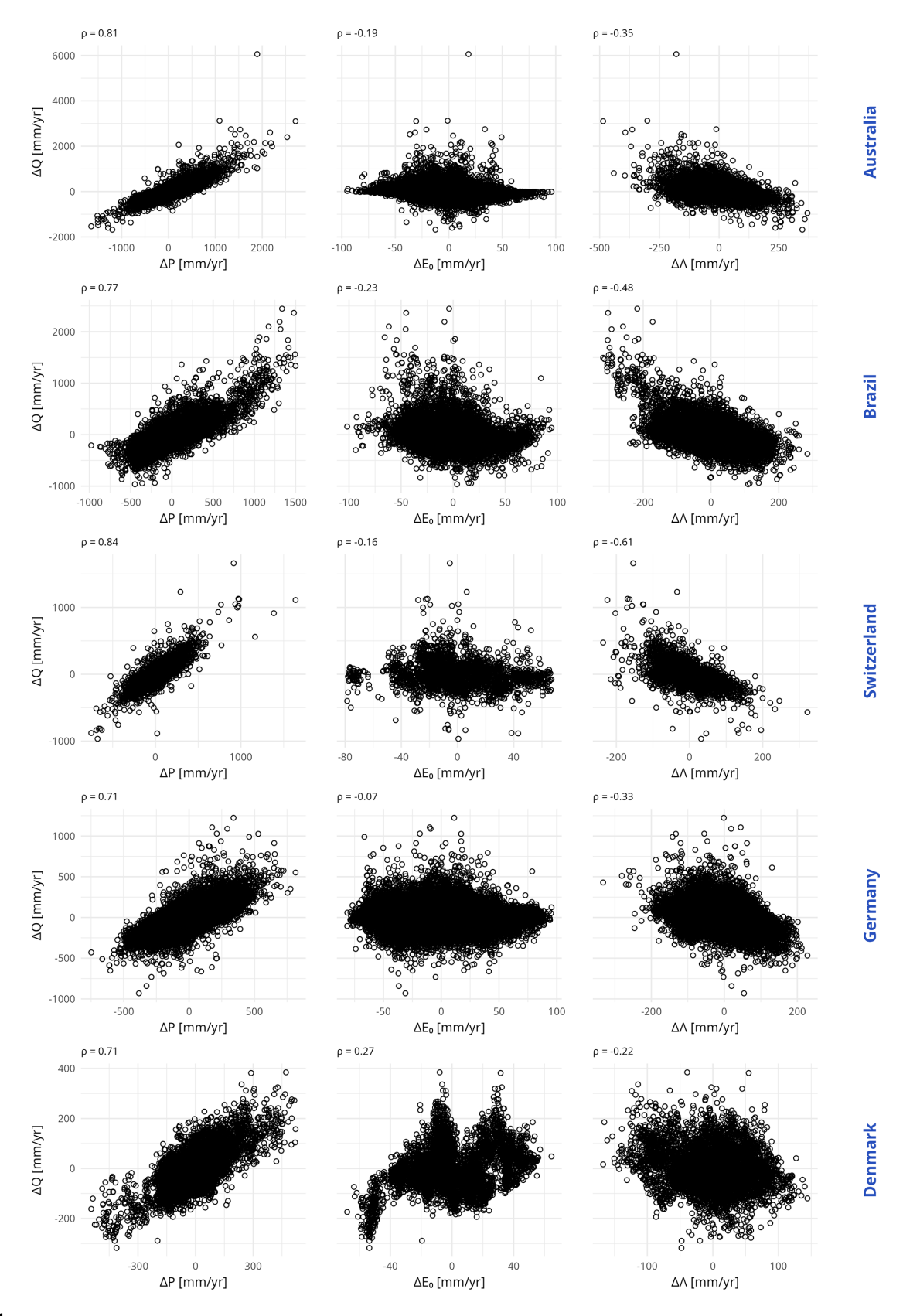


Figure 4.

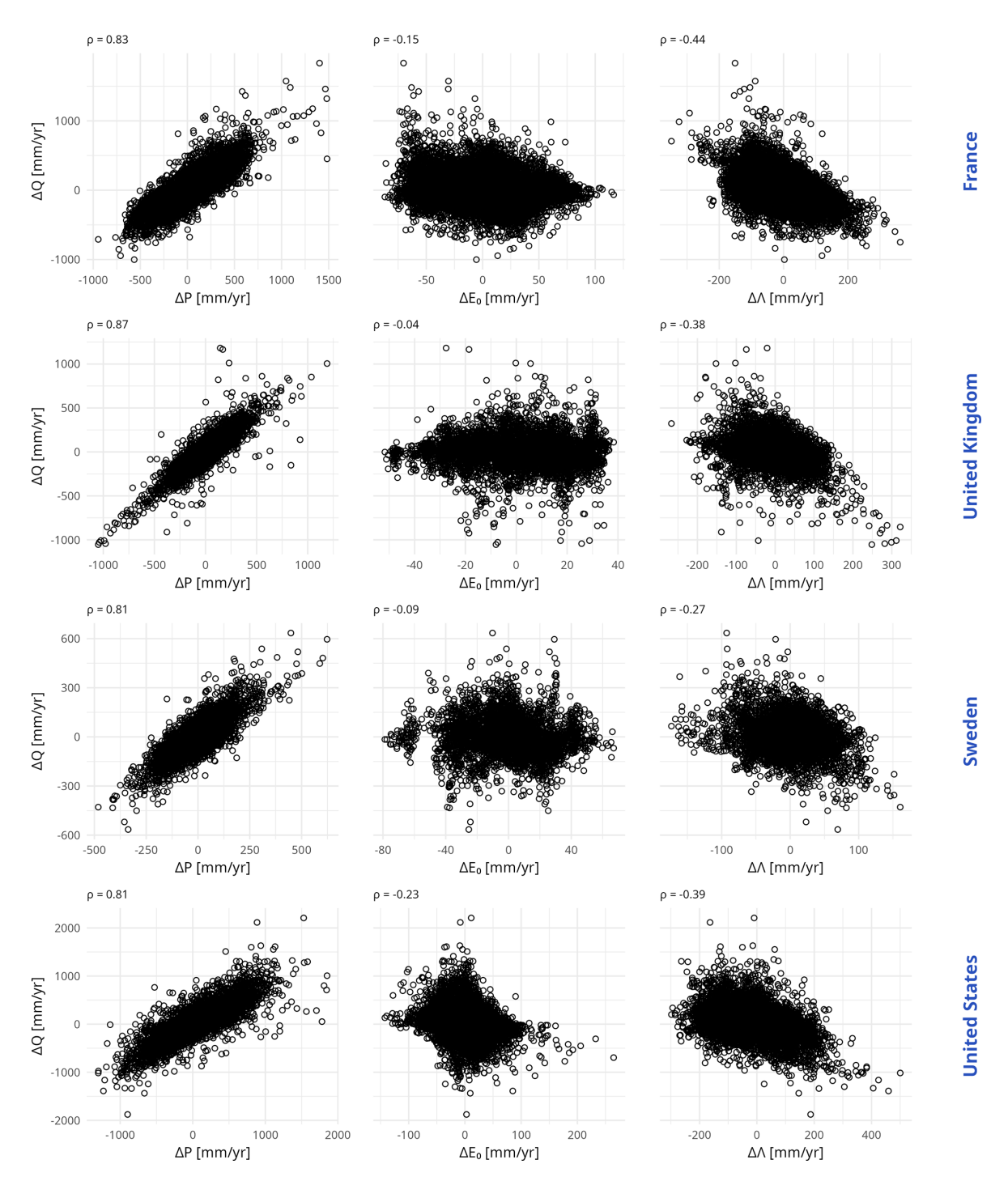


Figure 4. Scatter plots, for each country, between streamflow anomalies ΔQ , and: precipitation anomalies ΔP (left), potential evaporation anomalies ΔE_0 (middle) and synchronicity index anomalies $\Delta \Lambda$ (right). Each point represents one station-year. Above each scatter plot, we provide the corresponding Pearson correlation.

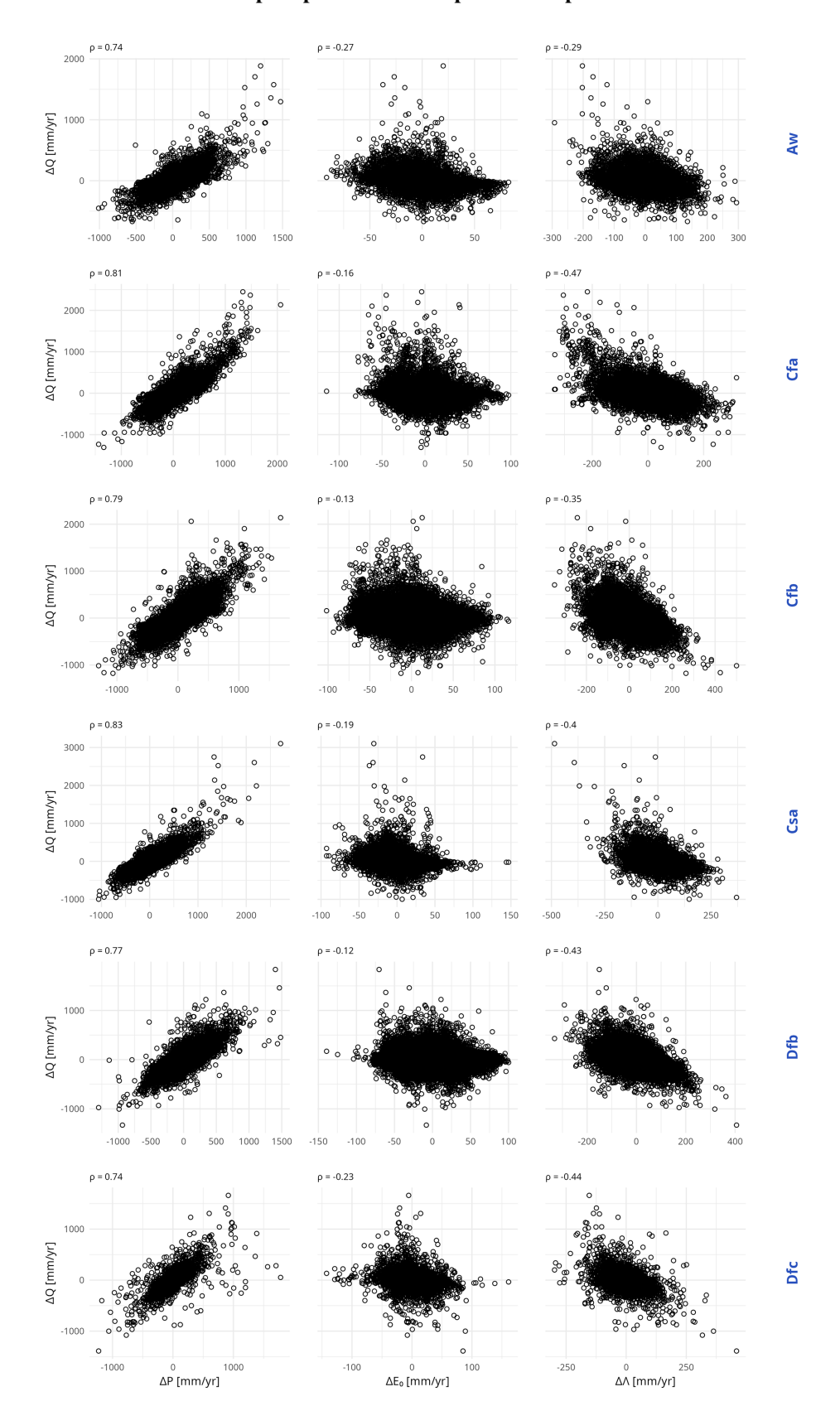


Figure 5. Scatter plots, for the main climate classes, between streamflow anomalies ΔQ , and: precipitation anomalies ΔP (left), potential evaporation anomalies ΔE_0 (middle) and synchronicity index anomalies $\Delta \Lambda$ (right). Each point represents one station-year. Above each scatter plot, we provide the corresponding Pearson correlation.

Table 4. Linear regression results by country and climate type for Eq. (6) when regression uses two independent variables P and E_0 to explain streamflow anomaly.

Mean adjusted R^2	e of catchments e_{Q/E_0} was	_	of catchments $e_{Q/P}$ was	_	Total number of catchments	Region or climate class
	significant and in the range $[-1,0]$	significant at the 0.05 level	significant and in the range [0,1]	significant at the 0.05 level		
						By country
0.67	9 %	18 %	97 %	100 %	546	Australia
0.61	4 %	12 %	86 %	95 %	636	Brazil
0.51	0 %	9 %	100 %	100%	202	Denmark
0.71	7 %	21 %	93 %	100%	628	France
0.47	9 %	18 %	93 %	94 %	1094	Germany
0.65	7 %	20 %	87 %	100 %	152	Sweden
0.75	0 %	8 %	86 %	100 %	73	Switzerland
0.75	2 %	25 %	89 %	99 %	136	UK
0.65	4 %	9 %	95 %	99 %	655	USA
					SS	By climate class
0.60	7 %	16 %	91 %	93 %	344	Aw
0.66	0 %	3 %	90 %	100 %	364	Cfa
0.60	7 %	18 %	94 %	98 %	1746	Cfb
0.67	1 %	7 %	96 %	99 %	196	Csa
0.56	9 %	21 %	94 %	96 %	956	Dfb
0.71	10 %	29 %	80 %	99 %	132	Dfc
0.61	6 %	16 %	93 %	97 %	4122	World

Aw – Tropical savanna climate with dry winter, Cfa – Temperate climate without dry season with hot summer, Cfb – Temperate climate without dry season with warm summer, Csa – Temperate climate with dry and hot summers, Dfb – Continental climate without dry season with warm summer, Dfc – Continental climate without dry season with cold summer

Table 5. Linear regression results by country and climate type for Eq. (7) when regression uses three independent variables to explain streamflow anomaly (to allow for comparison, the last column reports the mean R^2 of Table 4).

Country	Total number of catchments	Percentage of catchments where $e_{Q/P}$ was		Percentage of catchments where e_{Q/E_0} was		Percentage of catchments where $e_{Q/\Lambda}$ was		Mean adj. R^2	Mean adj. R^2 from Table 4
		significant at	significant and in	significant at	significant and in	significant at	significant and in		
		the 0.05 level	the range [0,1]	the 0.05 level	the range $[-1,0]$	the 0.05 level	the range $[-1,0]$		
By country									
Australia	546	100 %	98 %	38 %	20 %	87 %	83 %	0.76	0.67
Brazil	636	90 %	84 %	13 %	5 %	25 %	22 %	0.64	0.61
Denmark	202	100 %	100 %	6 %	0 %	44 %	44 %	0.56	0.51
France	628	100 %	96 %	30 %	13 %	82 %	79 %	0.77	0.71
Germany	1094	97 %	97 %	27 %	16 %	79 %	76 %	0.57	0.47
Sweden	152	100 %	90 %	24 %	5 %	41 %	38 %	0.69	0.65
Switzerland	73	96 %	82 %	8 %	0 %	22 %	21 %	0.76	0.75
UK	136	99 %	90 %	41 %	11 %	62 %	59 %	0.81	0.75
USA	655	99 %	96 %	11 %	5 %	57 %	52 %	0.71	0.65
By climate cl	ass								
Aw	344	90 %	88 %	18 %	10 %	42 %	40 %	0.67	0.60
Cfa	364	98 %	91 %	9 %	1 %	51 %	47 %	0.74	0.66
Cfb	1746	99 %	96 %	28 %	14 %	76 %	74 %	0.71	0.60
Csa	197	99 %	97 %	17 %	2 %	43 %	37 %	0.73	0.67
Dfb	956	98 %	96 %	27 %	14 %	68 %	65 %	0.66	0.56
Dfc	132	98 %	82 %	30 %	8 %	30 %	29 %	0.76	0.71
World	4122	97 %	94 %	23 %	11 %	64 %	61 %	0.67	0.61

Aw - Tropical savanna climate with dry winter, Cfa - Temperate climate without dry season with hot summer, Cfb - Temperate climate without dry season with warm summer, Csa - Temperate climate with dry and hot summers, Dfb - Continental climate without dry season with warm summer, Dfc - Continental climate without dry season with cold summer

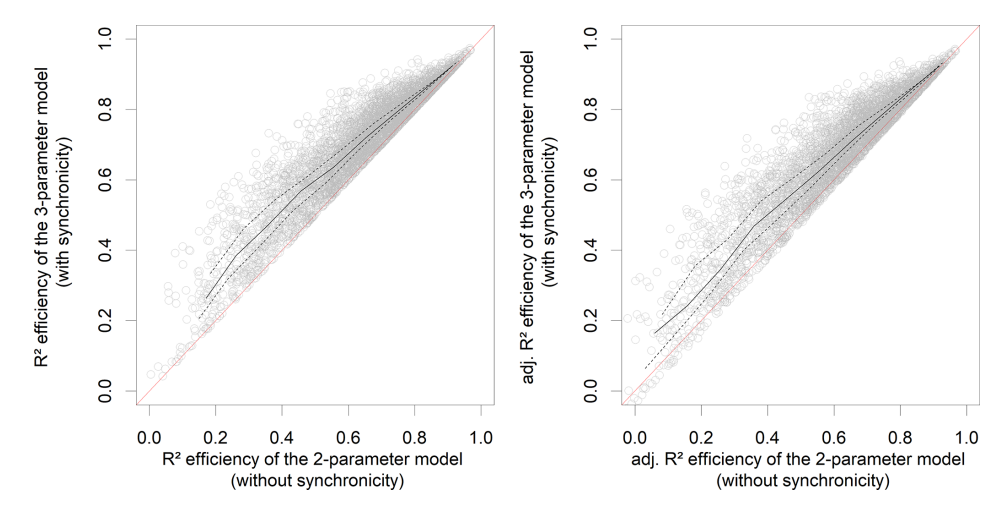


Figure 6. Comparison of the performances of the 2-parameter streamflow elasticity model (Eq. 6, which does not account for $P - E_0$ synchronicity) and the 3-parameter model (Eq. 7, which does). Each point represents one of the 4122 catchments of our dataset. The solid line represents the median, and the dashed lines represent the first and the third quartiles. As measure of efficiency, we use the R^2 on the left plot and the adjusted R^2 on the right one.

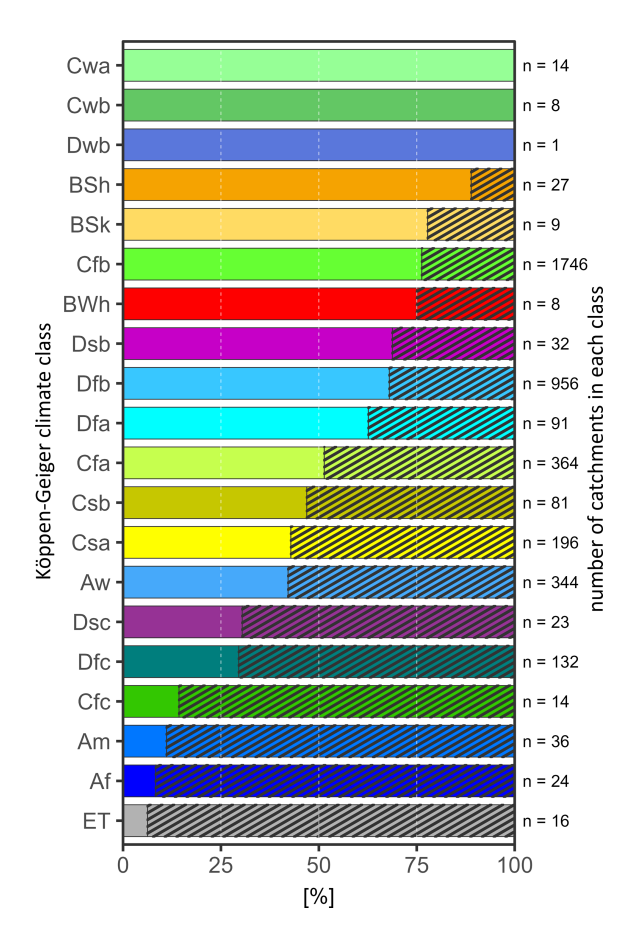


Figure 7. Significance of the $P - E_0$ synchronicity anomalies by Köppen climate class: the dashed area represents the proportion of catchments for which synchronicity was not deemed significant.

and potential evaporation, using a dataset of 4122 catchments located in Europe, Australia, North America and South America. Our analysis provided three main findings. First, we empirically verified the strong correlation among streamflow anomalies, annual precipitation anomalies, and synchronous $P - E_0$ anomalies. Second, we demonstrated that the role of the synchronicity between P and E_0 in explaining streamflow anomalies is significantly more important than that of E_0 anomalies. Finally, we showed that introducing synchronicity between precipitation and potential evaporation as an additional predictor in the linear regression clearly improves the prediction of annual streamflow variability.

6.2 Perspectives

Notwithstanding these positive results, some estimated elasticity values remain outside of their physically acceptable domain (i.e., [0,1] for $e_{Q/P}$ and [-1,0] for e_{Q/E_0} and $e_{Q/\Lambda}$). For precipitation elasticity $(e_{O/P})$, 93 % of the catchments were within the physical range, out of a total of 97 % where precipitation elasticity was significant. For potential evaporation elasticity (e_{Q/E_0}) , a lack of physical realism occurs in most of the cases (i.e., only 11 % of the catchments were within the physical range, out of a total of 23 % where potential evaporation elasticity was significant). This is very likely due to a sensitivity problem in the regression, which contributes to the difficulty in obtaining realistic elasticity coefficients. Finally, for synchronicity elasticity $(e_{O/\Lambda})$, 61 % of the catchments were within the physical range out of a total of 64 % where synchronicity elasticity was significant. In the future, we aim to investigate alternative statistical models that could better constrain the elasticity coefficients within their physically realistic domain.

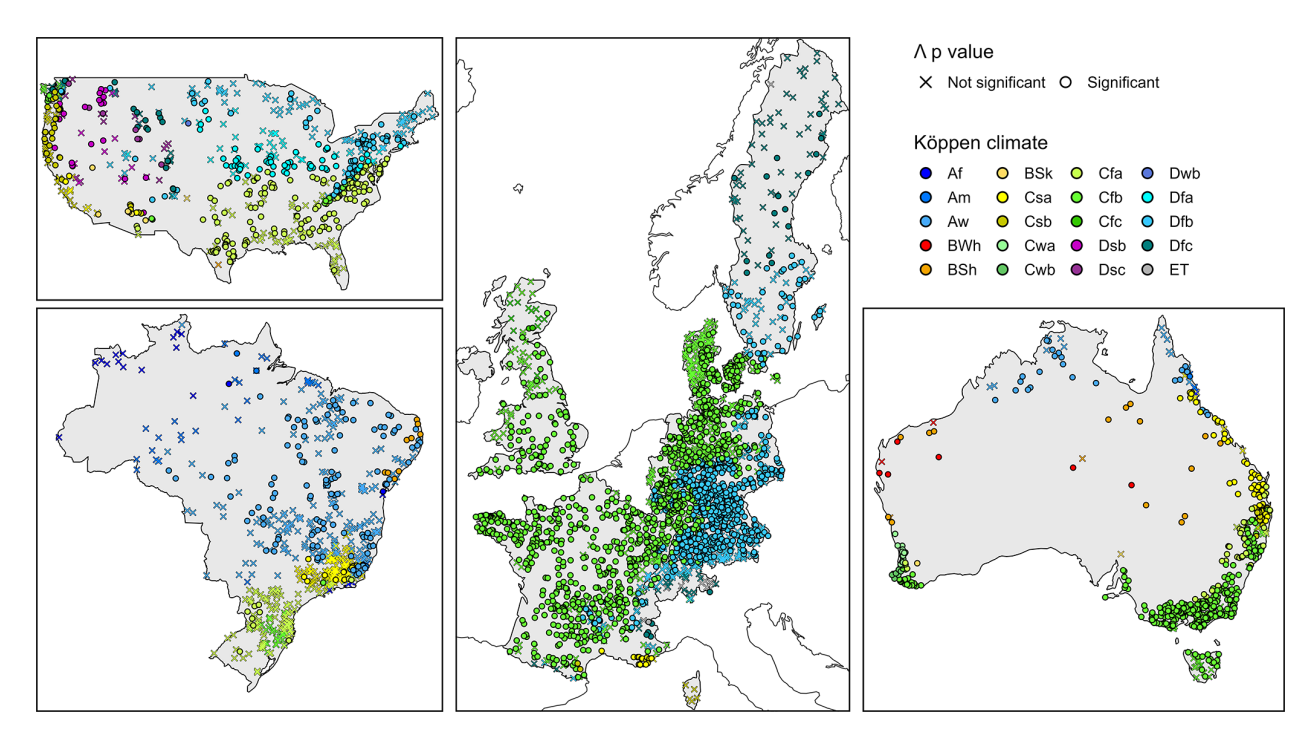


Figure 8. Map of the 4122 catchments used in this study, each catchment is represented by either a circle (where the $P-E_0$ synchronicity anomalies had a significant contribution to explain streamflow anomalies) or a cross (where it was not significant at the 0.05 level). The color of circles and crosses corresponds to the Köppen climate classes.

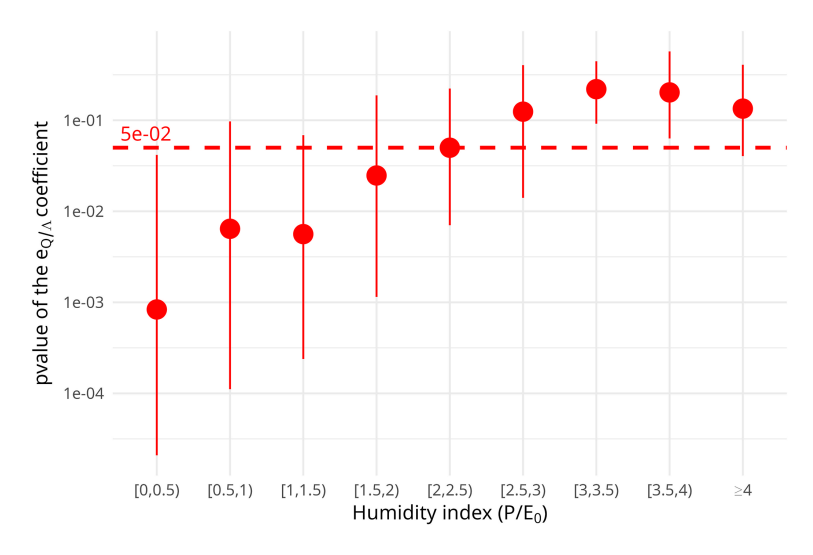


Figure 9. Distribution of the *p*-values of the 4122 $e_{Q/\Lambda}$ coefficients as a function of the humidity index P/E_0 . The red points represent the median, the bar represent the interquartile range, and the dashed line represents the 0.05 threshold.

Appendix A: Further details to justify our choice for the synchronicity index

There is no unique solution for choosing a measure of synchronicity between Precipitation and Potential Evaporation. In a previous paper (de Lavenne and Andréassian, 2018) we presented a non-dimensional index (λ) , defined as follows (A1):

$$\lambda = \frac{\sum_{m=1}^{12} \min(P_{m,n}, E_{0_{m,n}})}{\sum_{m=1}^{12} \max(P_{m,n}, E_{0_{m,n}})}$$
(A1)

A reviewer of this paper remarked that our interpretation of this index did not hold in extreme cases. Thus, we modified it in order to improve its interpretability. We also tried to replace it with simpler versions, and we would like to present these alternatives in order to save time and effort for those who would like to keep working on this topic.

The first simplification which was tested (called here S1) consisted in using directly the synchronous $P - E_0$ amount:

$$S1(n) = \sum_{m=1}^{12} \min(P_{m,n}, E_{0_{m,n}})$$
 (A2)

S1 was an interesting solution because it yielded directly a value in mm yr $^{-1}$, without the need for rescaling, and it clearly represented the precipitation volume that was the most easily accessible to evaporation. In the linear regression, it did give very high average adjusted R^2 (world average of 0.67, the same as for the solution retained). The reason why we did not consider this solution was that there was a correlation between $\Delta S1$ and ΔP for many catchments (average correlation of +0.58 over the 4122 catchments, reaching +0.74 over the Australian catchments), and introducing two correlated variables in a regression equation is clearly bad statistical practice.

To avoid this high correlation, we tested a normalization using annual precipitation, which we redimensionalized using the average interannual precipitation as in Eq. (A3) below:

$$S2(n) = \frac{\sum_{m=1}^{12} \min(P_{m,n}, E_{0_{m,n}})}{P_n} \cdot \bar{P}$$
 (A3)

The problem we found with S2 was that it yielded a constant value (equal to \bar{P}) for many arid catchments, where for most of the years $\frac{\sum_{m=1}^{12}(P_{m,n}\cap E_{0_{m,n}})}{P_n}=1$ because $P_{m,n}\ll E_{0_{m,n}}$.

We also tested a normalization using annual potential evaporation, which we redimensionalized using the average interannual potential evaporation as in Eq. (A4) below:

$$S3(n) = \frac{\sum_{m=1}^{12} \min(P_{m,n}, E_{0_{m,n}})}{E_{0_n}} \cdot \bar{E_0}$$
 (A4)

But S3 behaved similarly as S1 (clearly because the $\frac{\bar{E}_0}{E_{0n}}$ ratio is always close to 1), and the issue of having highly correlated values of $\Delta S3$ and ΔP reappeared.

This is why we finally opted for combining S2 and S3 using a geometric average (which correlation with the annual P is low: -0.10 on average), which was then redimensionalized using the average interannual precipitation. This yielded Λ_n , which has the desired dimension (mm yr⁻¹), and was used throughout this paper.

$$\Lambda_n = \frac{\sum_{m=1}^{12} \min(P_{m,n}, E_{0_{m,n}})}{\sqrt{P_n E_{0_n}}} \cdot \bar{P}$$
 (4)

Data availability. The data sources are listed in Table 1.

Author contributions. VA: conceptualization and writing, GMG: computations, figures, discussion, writing (review and editing), AL: computations, discussion, figures, JL: discussion, writing (review and editing).

Competing interests. The contact author has declared that none of the authors has any competing interests.

Disclaimer. Publisher's note: Copernicus Publications remains neutral with regard to jurisdictional claims made in the text, published maps, institutional affiliations, or any other geographical representation in this paper. While Copernicus Publications makes every effort to include appropriate place names, the final responsibility lies with the authors. Also, please note that this paper has not received English language copy-editing. Views expressed in the text are those of the authors and do not necessarily reflect the views of the publisher.

Acknowledgements. The authors would like to acknowledge the many individuals that worked to make available the hydrological datasets used in this paper. Special thanks are due to the two anonymous reviewers, to the Editor, as well as to Charles Perrin and Guillaume Thirel for their reviews and suggestions and to Laurent Strohmenger for his help with the Köppen-Geiger classification.

Financial support. This research has been funded in part by the Agence Nationale de la Recherche (projects CIPRHES ANR-20-CE04-0009 and DRHYM ANR-22-CE56-0007).

Review statement. This paper was edited by Mariano Moreno de las Heras and reviewed by two anonymous referees.

References

Addor, N., Newman, A. J., Mizukami, N., and Clark, M. P.: The CAMELS data set: catchment attributes and meteorology for

- large-sample studies, Hydrol. Earth Syst. Sci., 21, 5293–5313, https://doi.org/10.5194/hess-21-5293-2017, 2017.
- Almagro, A., Oliveira, P. T. S., Meira Neto, A. A., Roy, T., and Troch, P.: CABra: a novel large-sample dataset for Brazilian catchments, Hydrol. Earth Syst. Sci., 25, 3105–3135, https://doi.org/10.5194/hess-25-3105-2021, 2021.
- Andréassian, V., Coron, L., Lerat, J., and Le Moine, N.: Climate elasticity of streamflow revisited – an elasticity index based on long-term hydrometeorological records, Hydrol. Earth Syst. Sci., 20, 4503–4524, https://doi.org/10.5194/hess-20-4503-2016, 2016.
- Berghuijs, W. R., Sivapalan, M., Woods, R. A., and Savenije, H. H.: Patterns of similarity of seasonal water balances: A window into streamflow variability over a range of time scales, Water Resour. Res., 50, 5638–5661, https://doi.org/10.1002/2014WR015692, 2014.
- Chiew, F. H. S.: Estimation of rainfall elasticity of streamflow in Australia, Hydrol. Sci. J., 51, 613–625, https://doi.org/10.1623/hysj.51.4.613, 2006.
- Coutagne, A. and de Martonne, E.: De l'eau qui tombe à l'eau qui coule évaporation et déficit d'écoulement, IAHS Red Book series, 97–128, 1935.
- Coxon, G., Addor, N., Bloomfield, J. P., Freer, J., Fry, M., Hannaford, J., Howden, N. J. K., Lane, R., Lewis, M., Robinson, E. L., Wagener, T., and Woods, R.: CAMELS-GB: hydrometeorological time series and landscape attributes for 671 catchments in Great Britain, Earth Syst. Sci. Data, 12, 2459–2483, https://doi.org/10.5194/essd-12-2459-2020, 2020.
- Delaigue, O., Guimarães, G. M., Brigode, P., Génot, B., Perrin, C., Soubeyroux, J.-M., Janet, B., Addor, N., and Andréassian, V.: CAMELS-FR dataset: a large-sample hydroclimatic dataset for France to explore hydrological diversity and support model benchmarking, Earth Syst. Sci. Data, 17, 1461–1479, https://doi.org/10.5194/essd-17-1461-2025, 2025.
- de Lavenne, A. and Andréassian, V.: Impact of climate seasonality on catchment yield: a parameterization for commonly-used water balance formulas, J. Hydrol., 558, 266–274, https://doi.org/10.1016/j.jhydrol.2018.01.009, 2018.
- de Lavenne, A., Andréassian, V., Crochemore, L., Lindström, G., and Arheimer, B.: Quantifying multi-year hydrological memory with Catchment Forgetting Curves, Hydrol. Earth Syst. Sci., 26, 2715–2732, https://doi.org/10.5194/hess-26-2715-2022, 2022.
- Donohue, R., Roderick, M. L., and McVicar, T. R.: Roots, storms and soil pores: incorporating key ecohydrological processes into Budyko's hydrological model, J. Hydrol., 436–437, 35–50, https://doi.org/10.1016/j.jhydrol.2012.02.033, 2012.
- Dooge, J. C. I.: Sensitivity of runoff to climate change: A Hortonian approach, Bull. Am. Meteorol. Soc., 73, 2013–2024, https://doi.org/10.1175/1520-0477(1992)073<2013:SORTCC>2.0.CO;2, 1992.
- Feng, X., Vico, G., and Porporato, A.: On the effects of seasonality on soil water balance and plant growth, Water Resour. Res., 48, https://doi.org/10.1029/2011WR011263, 2012.
- Feng, X. Thompson, S. E., Woods, R., and Porporato, I.: Quantifying asynchronicity of precipitation and potential evapotranspiration in Mediterranean climates, Geophys. Res. Lett., https://doi.org/10.1029/2019GL085653, 2019.
- Fowler, K. J. A., Zhang, Z., and Hou, X.: CAMELS-AUS v2: updated hydrometeorological time series and landscape attributes

- for an enlarged set of catchments in Australia, Earth Syst. Sci. Data, 17, 4079–4095, https://doi.org/10.5194/essd-17-4079-2025, 2025.
- Hickel, K. and Zhang, L.: Estimating the impact of rainfall seasonality on mean annual water balance using a top-down approach, J. Hydrol., 331, 409–424, https://doi.org/10.1016/j.jhydrol.2006.05.028, 2006.
- Höge, M., Kauzlaric, M., Siber, R., Schönenberger, U., Horton, P., Schwanbeck, J., Floriancic, M. G., Viviroli, D., Wilhelm, S., Sikorska-Senoner, A. E., Addor, N., Brunner, M., Pool, S., Zappa, M., and Fenicia, F.: CAMELS-CH: hydro-meteorological time series and landscape attributes for 331 catchments in hydrologic Switzerland, Earth Syst. Sci. Data, 15, 5755–5784, https://doi.org/10.5194/essd-15-5755-2023, 2023.
- Jawitz, J. W., Klammler, H., and Reaver, N. G. F.: Climatic asynchrony and hydrologic inefficiency explain the global pattern of water availability, Geophys. Res. Lett., 49, e2022GL101214, https://doi.org/10.1029/2022GL101214, 2022.
- Koster, R. D. and Suarez, M. J.: A simple framework for examining the interannual variability of land surface moisture fluxes, J. Clim., 12, 1911–1917, https://doi.org/10.1175/1520-0442(1999)012<1911:ASFFET>2.0.CO;2, 1999.
- Leopold, L. B.: Water: A Primer, WH Freeman & Co, 172 pp., 1974.
 Loritz, R., Dolich, A., Acuña Espinoza, E., Ebeling, P., Guse, B., Götte, J., Hassler, S. K., Hauffe, C., Heidbüchel, I., Kiesel, J., Mälicke, M., Müller-Thomy, H., Stölzle, M., and Tarasova, L.: CAMELS-DE: hydro-meteorological time series and attributes for 1582 catchments in Germany, Earth Syst. Sci. Data, 16, 5625–5642, https://doi.org/10.5194/essd-16-5625-2024, 2024.
- Liu, J., Koch, J., Stisen, S., Troldborg, L., Højberg, A. L., Thodsen, H., Hansen, M. F. T., and Schneider, R. J. M.: CAMELS-DK: hydrometeorological time series and landscape attributes for 3330 Danish catchments with streamflow observations from 304 gauged stations, Earth Syst. Sci. Data, 17, 1551–1572, https://doi.org/10.5194/essd-17-1551-2025, 2025.
- Milly, P. C. D.: Climate, interseasonal storage of soil water, and the annual water balance, Adv. Water Resour., 17, 19–24, https://doi.org/10.1016/0309-1708(94)90020-5, 1994.
- Muelchi, R., Rössler, O., Schwanbeck, J., Weingartner, R., and Martius, O.: An ensemble of daily simulated runoff data (1981–2099) under climate change conditions for 93 catchments in Switzerland (Hydro-CH2018-Runoff ensemble), Geosci. Data J., 9, 46–57, https://doi.org/10.1002/gdj3.117, 2022.
- Oudin, L., Hervieu, F., Michel, C., Perrin, C., Andréassian, V., Anctil, F., and Loumagne, C.: Which potential evapotranspiration input for a rainfall-runoff model? Part 2 Towards a simple and efficient PE model for rainfall-runoff modelling, J. Hydrol., 303, 290–306, https://doi.org/10.1016/j.jhydrol.2004.08.026, 2005.
- Pardé, M.: Fleuves et rivières. Armand Colin, Paris, 224 pp., 1933a.
 Pardé, M.: L'abondance des cours d'eau, Revue de Géographie Alpine, 21, 497–542, https://doi.org/10.3406/rga.1933.5370, 1933b.
- Peel, M. C., Finlayson, B. L., and McMahon, T. A.: Updated world map of the Köppen-Geiger climate classification, Hydrol. Earth Syst. Sci., 11, 1633–1644, https://doi.org/10.5194/hess-11-1633-2007, 2007.
- Potter, N. J., Zhang, L., Milly, P. C. D., McMahon, T. A., and Jakeman, A. J.: Effects of rainfall seasonality and soil moisture capacity on mean annual water balance for Australian catchments,

- Water Resour. Res., 41, https://doi.org/10.1029/2004wr003697, 2005.
- Roderick, M. L. and Farquhar, G. D.: A simple framework for relating variations in runoff to variations in climatic conditions and catchment properties, Water Resour. Res., 47, https://doi.org/10.1029/2010WR009826, 2011.
- Sankarasubramanian, A., Vogel, R. M., and Limbrunner, J. F.: Climate elasticity of streamflow in the United States, Water Resour. Res., 37, 1771–1781, https://doi.org/10.1029/2000wr900330, 2001.
- Schaake, J. and Liu, C.: Development and application of simple water balance models to understand the relationship between climate and water resources, New Directions for Surface Water Modeling, IAHS Red Book series no. 181, 343–352, https://iahs.info/uploads/dms/7849.343-352-181-Schaake-Jr.pdf (last access: 1 October 2025), 1989.

- Thornthwaite, C. W.: An approach toward a rational classification of climate, Geog. Rev., 38, 55–94, https://doi.org/10.2307/210739, 1948.
- Turc, L.: The water balance of soils: relationship between precipitations, evaporation and flow [Le bilan d'eau des sols: relation entre les précipitations, l'évaporation et l'écoulement], Annales Agronomiques, Série A, 5, 491–595, 1954.
- Yokoo, Y., Sivapalan, M., and Oki, T.: Investigating the role of climate seasonality and landscape characteristics on mean annual and monthly water balances, J. Hydrol., 357, 255–269, https://doi.org/10.1016/j.jhydrol.2008.05.010, 2008.